JOURNAL PRE-PROOF

This is an early version of the article, published prior to copyediting, typesetting, and editorial correction. The manuscript has been accepted for publication and is now available online to ensure early dissemination, author visibility, and citation tracking prior to the formal issue publication.

It has not undergone final language verification, formatting, or technical editing by the journal's editorial team. Content is subject to change in the final Version of Record.

To differentiate this version, it is marked as "PRE-PROOF PUBLICATION" and should be cited with the provided DOI. A visible watermark on each page indicates its preliminary status.

The final version will appear in a regular issue of *Engineering Transactions*, with final metadata, layout, and pagination.

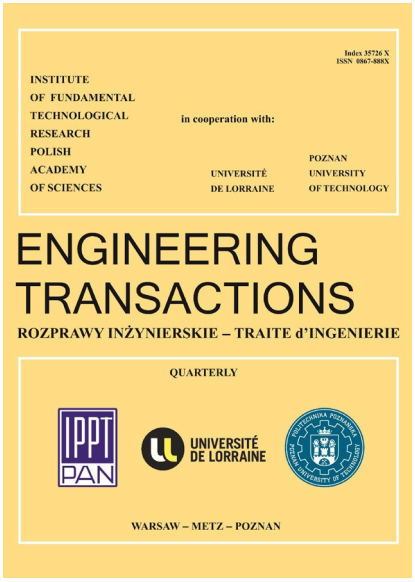

Title: Machine Learning-Based Welding Defect Recognition Using GLCM Features and k-fold Cross-Validation: KNN and SVM Techniques

Author(s): Sattar J. Kadhim, AbdulBaqi AlSalait, Raheem Al-Sabur, Abdel-Nasser Sharkawy

DOI: https://doi.org/10.24423/engtrans.2026.3652

Journal: *Engineering Transactions*

ISSN: 0867-888X, e-ISSN: 2450-8071

Publication status: In press

Received: 2025-09-06

Revised: 2026-03-05

Accepted: 2026-03-18

Published pre-proof: 2026-03-27

Please cite this article as:

Kadhim S.J., AlSalait A., Al-Sabur R., Sharkawy A.-N., Machine Learning-Based Welding Defect Recognition Using GLCM Features and k-fold Cross-Validation: KNN and SVM Techniques, *Engineering Transactions*, 2026, https://doi.org/10.24423/engtrans.2026.3652

Machine Learning-Based Welding Defect Recognition Using GLCM Features and k-fold Cross-Validation: KNN and SVM Techniques

Sattar J. Kadhim[1,a], **AbdulBaqi AlSalait**[2,b] , **Raheem Al-Sabur**[1,c,*], **and Abdel-Nasser Sharkawy**[3,4,d]

[1]Mechanical Engineering Department, University of Basrah, Basrah 61004, Iraq
[2] Consultant of Energy Affairs, Ministry of Oil, Government of Iraq
[3]Mechanical Engineering Department, Faculty of Engineering, Qena University, Qena 83523, Egypt
[4]Mechanical Engineering Department, College of Engineering, Fahad Bin Sultan University, Tabuk 47721, Saudi Arabia
Emails: hasansatar2002@gmail.com[a], raheem.musawel@uobasrah.edu.iq[c], abdulbakiuof@yahoo.com[b], abdelnassersharkawy@eng.svu.edu.eg[d]

Abstract

Although radiographic inspection is one of the oldest techniques for non-destructive testing, it is still considered vital in many industrial fields to ensure the quality of welds and meet the demands of work conditions and design, as well as safety and reliability requirements. This paper presents an algorithm that identifies and categorizes welding defects in radiographic images using machine learning techniques. For this aim, two supervised classifiers are proposed and performed, which are 1) K-nearest Neighbour (KNN), which is a nonparametric classifier, and 2) a multiclass classifier based on Support Vector Machine (SVM) as an intensive learning-based classifier (enthusiastically learns). SVM is commonly used in binary classification, but it can be adapted for multi-classification using various common methods, such as one-versus-one and one-versus-all. The texture features are adopted in this paper as inputs to the classifiers, where two groups of them are used: the feature of the Local Binary Pattern (LBP) and the grey-level co-occurrence extraction matrix (GLCM), to obtain the feature vector. To avoid the risk of overfitting, four k-fold cross-validations are applied. The experimental results are reported for two different classifiers, achieving an accuracy of 91.66% when combining GLCM and SVM.

Keywords: *Welding defect; Radiographic images; Classification; Machine Learning; k-fold cross-validation*

1. Introduction

1.1 Background

To ensure the quality of welding, the traditional approach in welding environments involves using non-destructive testing (NDT) and post-weld techniques for evaluation. In welding fields, the main nondestructive tests can be categories as: visual inspection (VT) [1], ultrasonic

testing (UT) , radiographic testing (RT) [2], eddy current testing (ECT) [3], magnetic particle testing (MT)[4], liquid penetrant testing (PT)[5], acoustic emission testing (AE)[6], infrared thermography (IRT)[7], stereography[8], and computed tomography (CT) [9]. X-ray as a radiography test can be used on a variety of materials with varying densities, as it can penetrate a wide range of materials to detect internal faults in welds [10]. Defective regions absorb greater amounts of energy, which results in a dimmer appearance. Among the most popular flaws that are possible to detect in the images of radiographic inspection are porosity (the defect that arises from the entrapment of gas), lack of fusion (the defect as a result of the lack of union between the base metal and welding), cracks (interruptions that are fractures in the metal), solid inclusions (the defect that arises from foreign matter which is trapped during welding), burn-through (penetration of the welding metal at the root zone of the base metal due to excessive heat), and lack of penetration (penetration less than specified is usually existing at the root of the weld) [11], [12], [13].

1.2 Related Work

The detection and classification of welding flaws are crucial in real-life and industrial environments. Furthermore, it is considered one of the most important research topics that has been investigated. Liao and Ni's study is considered a pioneer in the use of digital radiographs to identify weld defects by comparing pixel intensities with a Gaussian pattern in the weld region [14]. They demonstrated that similarity can be measured by the mean square error (MSE), with the lowest MSE indicating a weld line. A method was developed that focuses on the geometric features of flaws to improve the accuracy of welding defect detection using linear classifiers. It was found that having high-quality features is more important than simply having a large number of features for reliable classification[15]. Tuo et al. [16] yielded a higher accuracy when using the Gabor filter and the Grey-Level Co-occurrence Matrix (GLCM) in welding defect classification. They applied principal component analysis (PCA) to minimize the feature vector dimensions and used K-nearest neighbours (KNN) as a comparison classifier. In the last twenty years, researchers have turned more and more to the Gray-Level Co-Occurrence Matrix (GLCM) as a practical way to study weld images [17], [18], [19]. By pulling out texture features, it has helped make defect detection faster and more accurate, while cutting down on the need for manual inspection. A Gabor filter to characterize texture features in an automatic system for detecting weld discontinuities, as feature extraction focuses primarily on calculating the properties of areas. Consequently, the former displays the number of occurrences of a specific grey value in relation to another grey value in the image and in a specific spatial context by the user [20]. The application of the Gabor filter and GLCM was extended in welding defect classification by applying the SVM algorithms and the receiver operating characteristic (ROC) curve [21]. This modification enabled the study of features' morphology, such as the size and shape of defects.

Artificial Neural Networks (ANNs) have made an influential contribution to the diagnosis of weld defects based on digital images of radiographic tests, and their results have shown increasing reliability and promising validity [22]. ANNs have become increasingly popular in conjunction with other classification methods, such as KNN and Support Vector Machine (SVM), to differentiate welding flaws in images from radiographic testing. Both morphological

and texture features are adopted to implement the segmentation process and generate the feature vector in the classification system procedure [23]. More modifications achieved using deep ANNs to classify the defects of welding in images of radiographic tests reached around 75.83% to 98.75% [24]. This algorithm enables the classification of defects into more categories, including non-penetration, crack, pore, and no-defect status. Later, by applying the deep learning algorithm pipelines for welding defects, the defect categories were extended to include seven flaws: porosity, undercut, crack, inclusion of slag, lack of penetration, lack of fusion, and interior concavity [25].

1.3 Main Contributions and Outline

Based on the above discussion, further investigation into the detection and classification of weld flaws from images is warranted. Using machine learning and new advanced methods is worthy of studying and evaluation. Furthermore, obtaining very high performance (accuracy, precision, and recall) for the model is the top priority.

The main contribution of this study is presented in the following points:

- An advanced algorithm that exploits machine learning is proposed to detect and classify weld flaws from images with a very high performance (accuracy, precision, and recall).
- The proposed algorithm involves capturing images with an ordinary digital camera, enhancing them to remove noise using a common filter, such as the adaptive median filter, and basing the classification on the texture that describes the attributes, as it has shown very high effectiveness.
- This is accomplished more specifically by utilizing the feature descriptors of the local binary pattern (LBP) and grey level co-occurrence matrices (GLCM), after which the classification process commences.
- For classifiers, their selection is made using two methods of machine learning: a multiclass classification based on SVM and K-nearest neighbours (KNN). Thus, it is possible to dispense using specialized equipment or skilled workers who have experience and knowledge in the field of inspections.

The rest of the sections of this paper are outlined as follows. **Section 2** presents the proposed methodology in this paper, including the proposed methods, the collected dataset, the classification process, and the evaluation metrics. In **Section 3**, the experimental results are presented and discussed. In **Section 4**, the paper's main points are summarized, and some future work is highlighted.

2. Materials and Methods

2.1 Datasets Preparation

Film digitization is an important step in the system used to determine welding defects. As a result, the most important factors for the performance of the above-mentioned system are the choice of an optimized scanning accuracy and an acceptable level of digitization quality. Radiographic film digitization is carried out using several systems based on American Society

of Mechanical Engineers (ASME) standards. The most common method is scanning, which uses light transmission (transparency adapters). The dataset images were captured with a Nikon D7000 digital camera, tuned to achieve optimal contrast. Indeed, the Nikon D7000 camera can be used for radiography using a technique called indirect digital radiography. This entails taking pictures of an X-ray-exposed fluorescent screen using the camera. The camera was set up at a location with a 400 mm lens, without a flash. Dataset images are prepared by converting them from RGB to greyscale and automatically cropping them. This step highlights the welding area and a limited surrounding area. The symbols, numbers, and cues that are often associated with welding films are eliminated. Next, preprocessing models and approaches are used to minimize noise and enhance contrast, allowing the main objects in the image to be distinguished from the background, making them more discernible. Once segmentation is completed, the two extractors of feature texture (LBP and GLCM) are performed to choose the features that are strongly distinctive for the classifiers. An automated system for identifying, recognizing, and classifying the welding defects was developed using two proposed classifiers; 1) Error Correcting Output Coding (ECOC) with SVM and 2) KNN. The features and weld fault identification can be obtained from these two proposed classifiers. This proposed methodology is presented in **Fig. 1**.

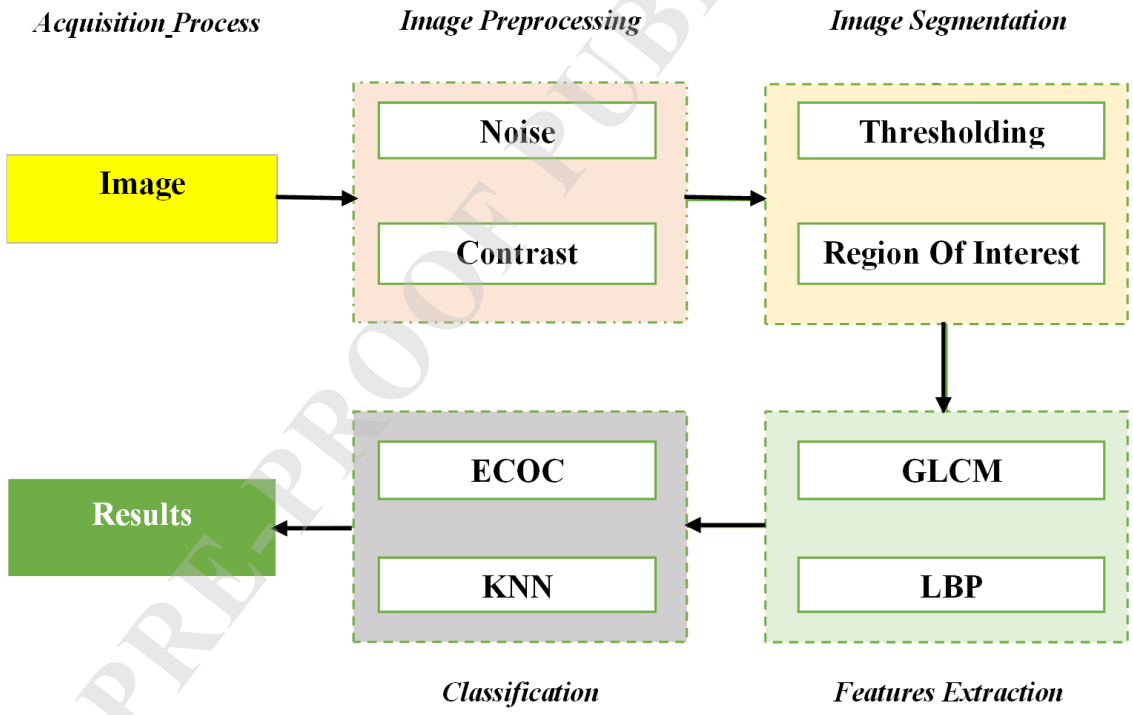

Fig. 1. Procedure for classifying welding defects. (ECOC is the SVM learner).

The total number of images in the data set is 72. The images are used to cover four types of defects, which are distributed among burn-through (BT), solid inclusions (SI), concavity (CO), and incomplete penetration (IP), as shown in **Table 1**. Experts in the field of radiograph interpretation establish previous knowledge about these images. Sampling images containing BT is presented in **Fig. 2**.

Table 1. Dataset of welding defects radiographic images.

Welding Defect	No. of images
Solid Inclusions (SI)	25
Burn-Through (BT)	17
Incomplete Penetration (IP)	22
Concavity (CO)	8

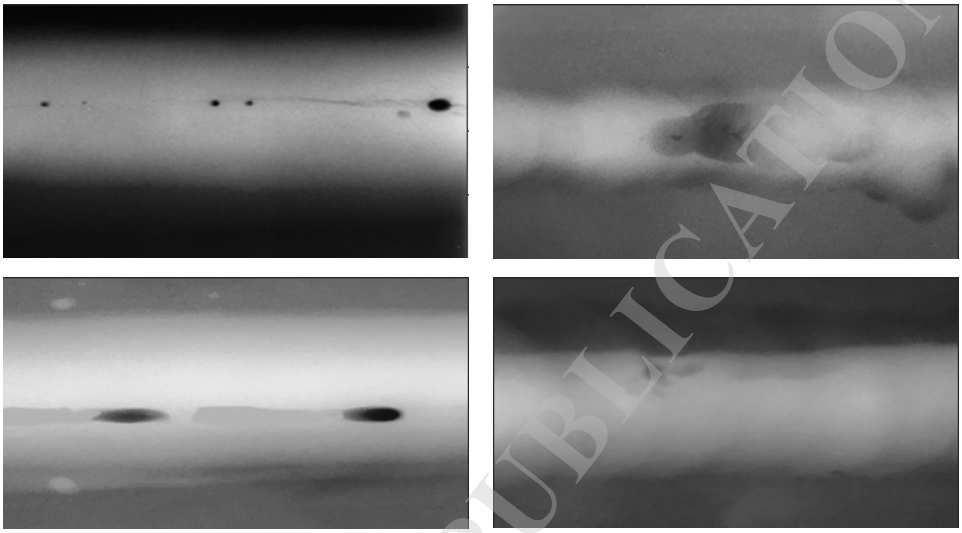

Fig. 2. Sampling images contain burn through (BT). This Figure is one of the photographs of our dataset.

2.2 Image preprocessing

As a system of imaging, the non-destructive testing (NDT) image nature is affected by a signal, which is arbitrary and named as the noise. This signal is always appearing during the process of image capture, which includes coding, image transmission, and processing steps [26].

The presence of this noise could disorganize the primary data of the images of radiography. The exporter of noise in digital images can cause problems and be considered a defective device in the data acquisition process. The process of filtering is a crucial and essential step in image preprocessing [27], [28]. Additionally, this process can improve the quality of the images. The primary function of the image filtering process is to remove damage and noise from the image, thereby achieving a high-quality image.

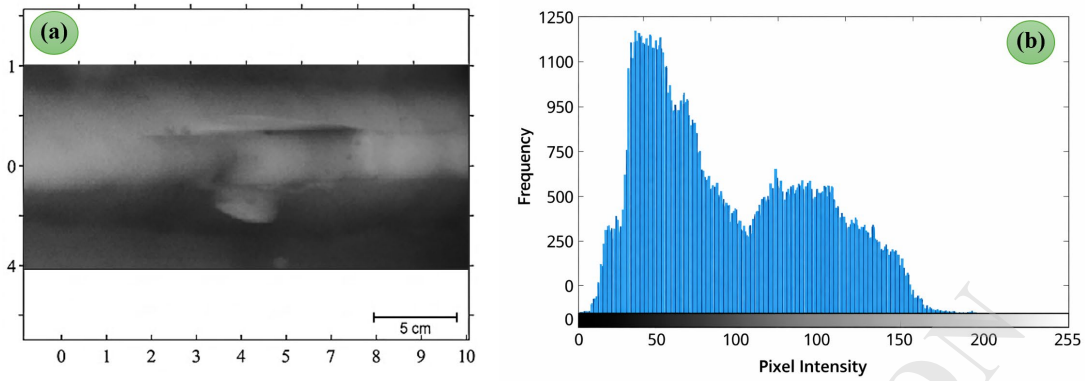

(a) Original image (b) Histogram of original image

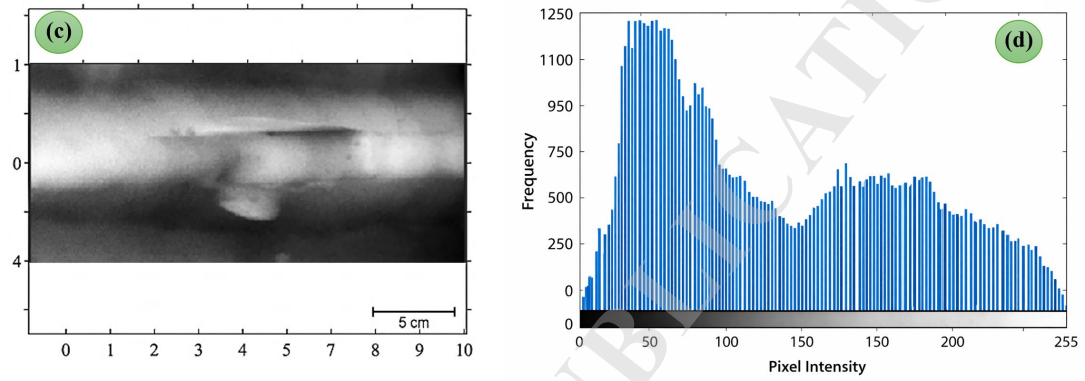

(c) Stretching image (d) Histogram of stretching image

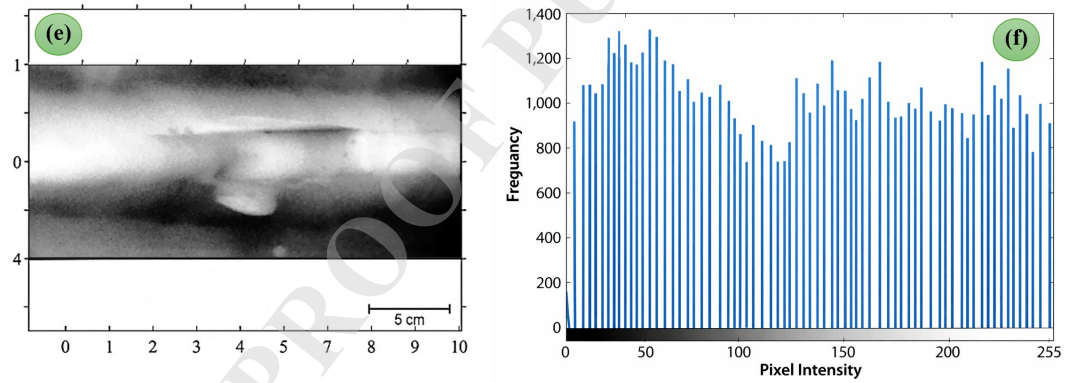

(e) Global equalization image (f) Histogram global equalization

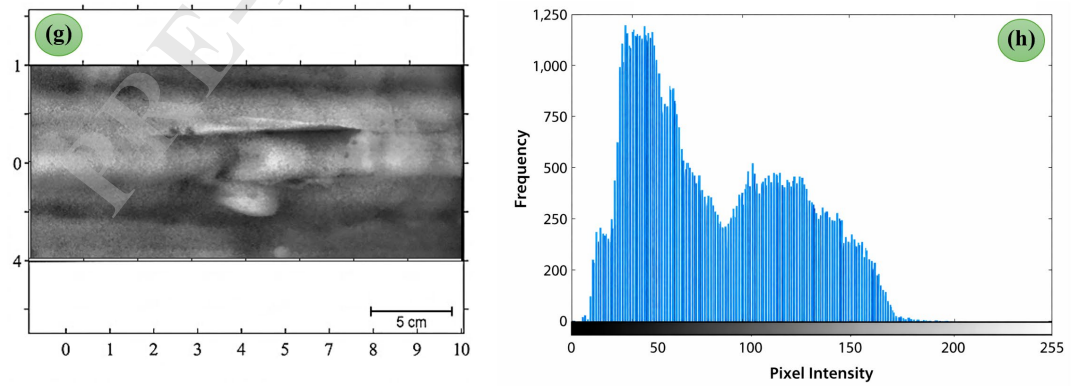

(g) Local equalization image (h) Histogram of CLAHE

Fig. 3. Various improvement techniques carried out on an image with incomplete penetration. This Figure is one of the photographs of our dataset.

Image contrast refers to a type of image manipulation that modifies and improves the image's appearance [29], [30]. It can be defined as the dynamic range measure, which represents the entire range of intensity that values found in the image. In another definition, it can be the difference between the maximum and minimum pixel values. A histogram is an essential tool to know whether an image has a large or small dynamic range. Therefore, for high contrast, the histogram should be extended to encompass the entire dynamic range. Examples of radiographic images and image brightness improvement using different methods are presented in **Fig. 3**. The left side indicates that the original images of incomplete penetration that were stretched, then global and local equalized, while the right side explores the histogram of the corresponding cases. All these improvement methods are applied on the images to find the one which gives the higher performance. The best performance is obtained by method of stretching.

2.3 Image Segmentation

Segmentation can be described as dividing images into parts based on specified rules. These parts or areas can be considered homogeneous in certain visual aspects, such as color or density [31], [32]. The most effective and efficient technique for segmenting and classifying images of welding inspection films is the thresholding technique [33], [34]. An example of the segmentation process by different thresholding techniques is presented in **Fig. 4**. The original image **(Fig. 4a)** was adaptive thresholding **(Fig. 4b)**, then global thresholding **(Fig. 4c)**, and histogram thresholding **(Fig. 4d)**. All these segmentations methods are applied on the image. The best performance is obtained by adaptive thresholding.

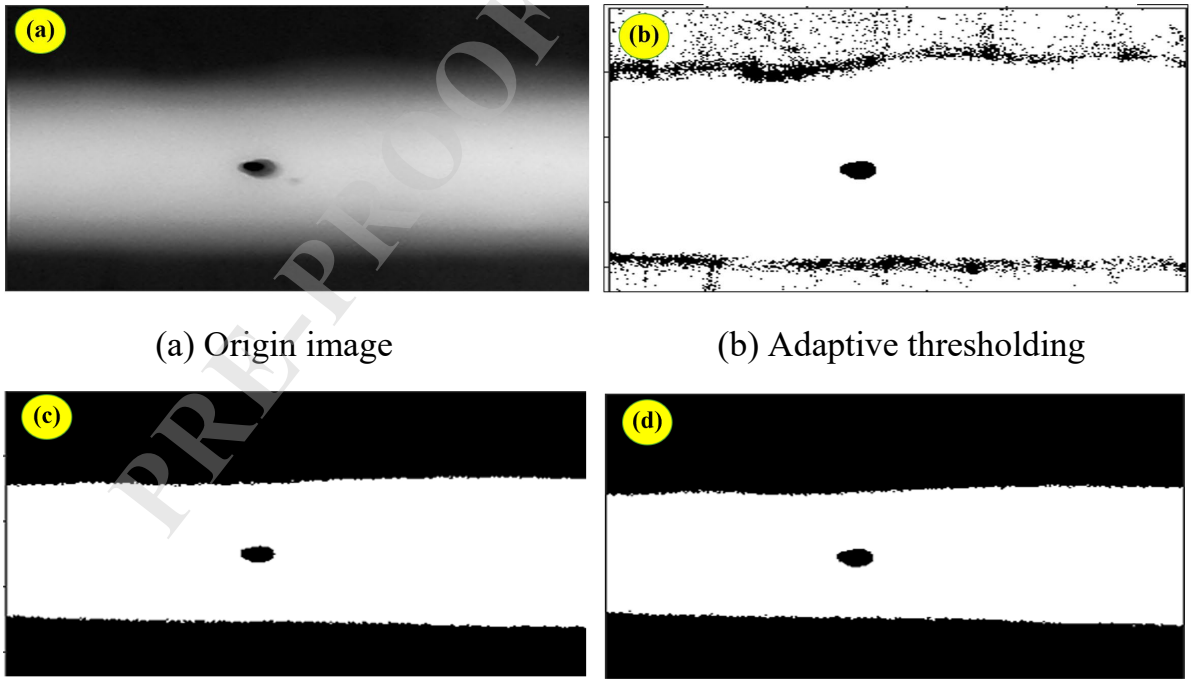

Fig. 4. Segmentation process by different thresholding techniques. This Figure is one of the photographs of our dataset.

2.4 Gray-level co-occurrence extraction matrix (GLCM)

This method is a statistical approach to analyzing grey level values by examining their spatial distribution in images, which effectively identifies distinguishing characteristics that can be used to find texture-related features [35], [36], [37]. The method can be summarized by creating a matrix that aggregates the total number of pixel pairs in the image. It represents the evaluation of a frequency of two grey levels within a specified region. GLCM reveals a specific relationship of several times that occur between adjacent pixels (reflects the correlation between two adjacent pixels within a local region). The creation of the matrices depends on both the distance and the direction. It shows that the reference pixel of intensity (i) has special relevance with the adjacent pixel of intensity (j), which is separated by a spatial distance of (d) and a direction of (θ). Many ways exist for determining the spatial relationship between two neighboring pixels, considering different angles and displacements. This is clear in **Fig. 5**. After the matrix has been created, many statistics are derived and can be applied to the GLCM. As the number of statistics reaches fourteen, statistical tasks are characterized by accuracy. The most widely used ones are variance, energy, homogeneity, and correlation on a large scale [38].

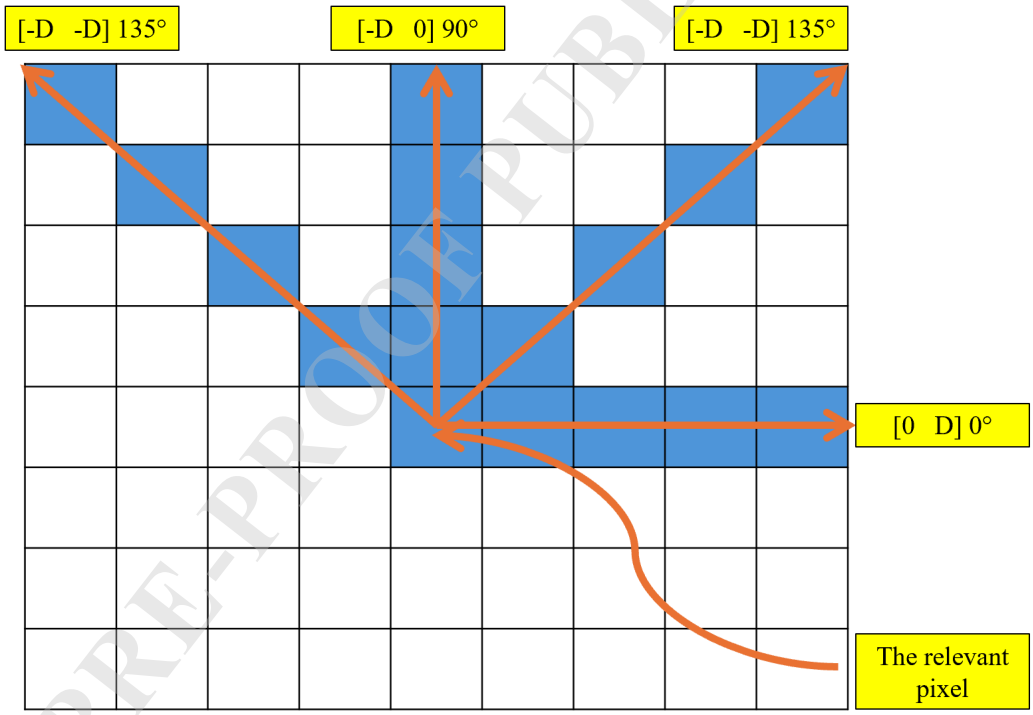

Fig. 5. Different co-occurrence matrix offset to extract the features of texture.

2.5 Local Binary Pattern (LBP)

This factor determines the texture of the image and is based on the difference in pixel values near it. In the analysis of textiles, this factor presents a significant leap and is preferable compared to other previous techniques in various applications, as it has undergone substantial development and progress [39], [40], [41]. The local binary pattern is creative tool to texture

classification [42]. The main idea of this pattern is that it depends on being a descriptor, using two scales, which are the local patterns and the grey contrast. A local binary code is extracted for each pixel found in the image by assigning the neighboring pixels with the value of the center pixel, which shows the threshold.

This illustrates the neighborhood by multiplying the threshold by the corresponding pixel-specific weight. Therefore, a histogram is created to combine the iterations of the different binary patterns. The base operator model reveals that it depends on the eight neighboring pixels around the pixel in question [43]. The details of the texture of LBP are obtained originally from a 3 x 3 window by the use of the grey value of the neighboring pixels as a threshold. **Fig. 6** shows the LBP operator basic.

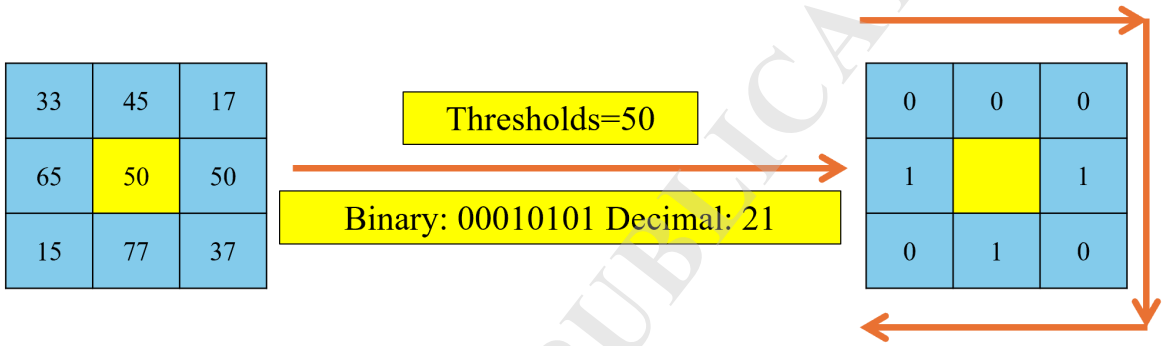

Fig. 6. Basic LBP operator.

2.6 Classification

The ability to create a model or an approach that can identify the different categories in a data set. Based on the results obtained from the training process, many outputs can be predicted. Moreover, there is a possibility of classifying these predicted data. In this study, the k-nearest neighbors (k-NN) algorithm and the support vector machine (SVM) algorithm were used as classifiers during testing, which are well-suited for handling non-linear issues [44], [45], [46].

2.7 Multiclass SVM classification

Various methods have been proposed to utilize SVM for handling multi-class problems, as it can be extended by merging multiple of its types into a multi-class classifier [47]. For the present multi-class classification schemes, the one-against-all model (OAA) is the most commonly used. Classification functions are built between each category relative to the remaining categories. An M-class problem is modified into M dual-category problems. Using the entire training data to perform the learning step of the classifiers, on the basis that the data vectors from a certain category are positive and all other samples are negative. In the testing step, classification is performed by calculating the margin from the linear separating hyperplane. The class with the maximum decision value is the final output. A merit of this method is that the number of binary classifiers to build is equal to the number of categories. According to the maximum output value of the SVM classifiers, the label of an instance is predicted. One drawback of the one-to-all approach is that the dataset is significantly unbalanced after collecting the M-1 categories [48], [49], [50].

Another approach is to build a group of one-versus-one classifiers, where the imbalance is less pronounced in the dataset than in the previous method, by separating the M-class dataset problem into multiple binary classification problems (M-1) / 2 and fitting a binary classification model on each. This method appears to be overly complex, as the number of classifiers obtained is often too large, and the model is too intricate. Consequently, this model is not suitable for solving problems that contain a large number of categories. However, if the number of categories is not very abundant, each binary class is trained on a smaller amount of data. As a result, the training and tuning process of the classifier becomes more efficient and faster. To determine the class of an unknown sample, the obtained M (M-1)/2 binary classifiers are used, and the class containing the most common object samples is predicted through the voting method [48].

2.8 Evaluation Metrices

To assess the quality of the classifier, a confusion matrix is used, which provides a visual representation of its predictive power. This matrix, as shown in **Fig. 7**, [51], includes the following classes: true positive, true negative, false positive, and false negative. These classes are defined as follows:

- True-Positive (TP) means the classifier predicts positive and it is positive in fact.
- True-Negative (TN) means the classifier predicts negative and it is negative in fact.
- False-Positive (FP) means the classifier predicts positive and it is negative in fact.
- False-Negative (FN) means the classifier predicts negative and it is positive in fact.

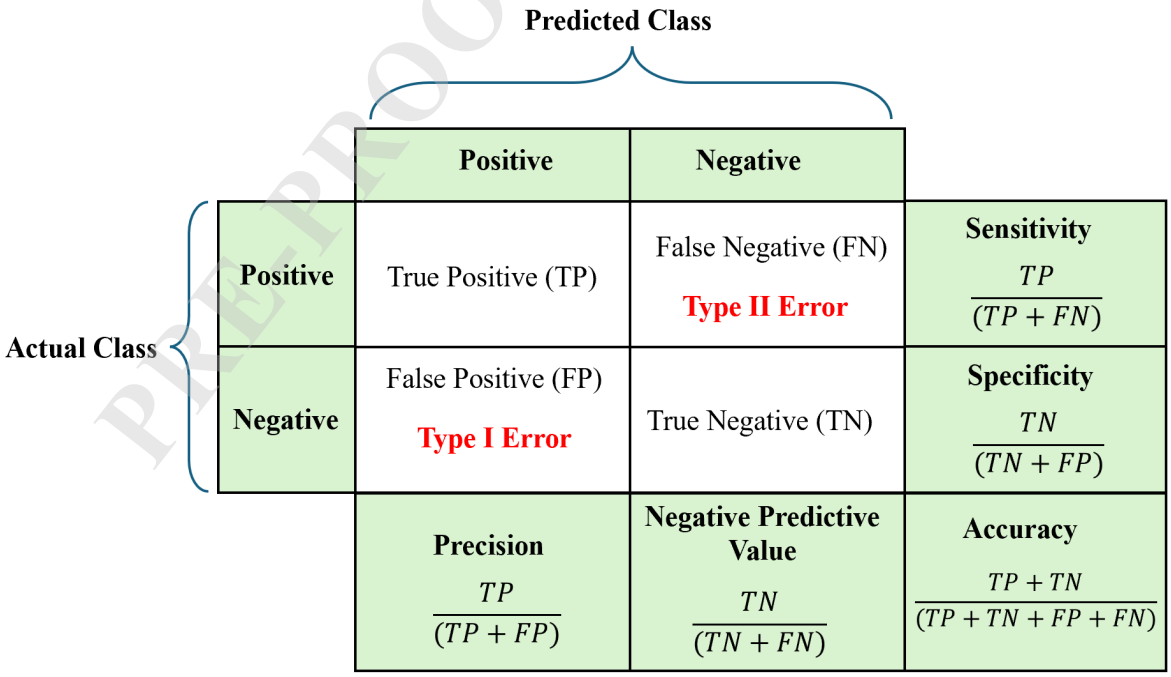

Fig. 7. The confusion matrix structure, [51].

The main measures presented in the confusion matrix is discussed. Accuracy measures the closeness of the quantity to the actual/real value. It is considered a very effective metric if relatively symmetric dataset is found, [52], [53].

$$Accuracy = \frac{correct\ prediction}{tatal\ dataset} = \frac{TP+TN}{TP+TN+FP+FN} \quad (1)$$

Measuring the percentage of correct predictions made by the proposed model is the precision. It is defined by dividing the positive examples' number that are correctly classified by all the examples that classifies as positive by the classifier. The following form can represent it:

$$Precision = \frac{TP}{TP+FP} \quad (2)$$

The third metric is recall which indicates the percentage of all potential ground truth boxes identified. It is expressed as the number of correctly categorised positive examples divided by the total number of positive examples in the data, [52].

$$Recall = \frac{TP}{TP+FN} \quad (3)$$

The experimental results from applying the proposed classifiers are presented in the next section.

3. Experimental Results

Different settings for GLCM are explored to identify the features most suitable for the classifier by conducting multiple tests that vary both distance and direction. Four directions are considered in the current work as follows: 0°, 45°, 90°, and 135°, with a spatial distance set to neighbour two pixels. The settings for both direction and distance for constructing GLCM are presented in **Table 2**.

Table 2. Setting of distance and direction for the GLCM construction.

Parameter	**Setting**				
Item	1	2	3	4	5
Direction &Angle	[0 2] (to east)	[-2 2] (to northeast)	[-2 0] (to north)	[-2 -2] (to northwest)	Combination of items (1&2)
Features No.	10	10	10	10	10 + 10 = 20
Features	Angular Second Moment, Energy, Entropy, Contrast, Max. Probability, Dissimilarity, Homogeneity, and GLCM Mean, Variance and Correlation				

The interpretion of all GLCM features incorporated in the current work is presented in **Table 3**.

Table 3. Description and visualization of all GLCM features or offests incoportated in this current work.

Offset	Distance (d) in pixels	Direction (θ)	Description
GLCM [0 1]	1	0° (Horizontal)	Neighbor is 1 pixel to the right
GLCM [0 2]	2	0° (Horizontal)	Neighbor is 2 pixels to the right
GLCM [-1 1]	$\sqrt{2}$	45° (Diagonal)	Neighbor is 1 pixel up and 1 pixel right
GLCM [-2 2]	$2\sqrt{2}$	45° (Diagonal)	Neighbor is 2 pixels up and 2 pixels right
GLCM [-1 0]	1	90° (Vertical)	Neighbor is 1 pixel up
GLCM [-2 0]	2	90° (Vertical)	Neighbor is 2 pixels up
GLCM [-1 -1]	$\sqrt{2}$	135° (Anti-diagonal)	Neighbor is 1 pixel up and 1 pixel left
GLCM [-2 -2]	$2\sqrt{2}$	135° (Anti-diagonal)	Neighbor is 2 pixels up and 2 pixels left

It should be noted that GLCM features; GLCM [0 2], GLCM [-2 2], GLCM [-2 0], and GLCM [-2 -2] are used for SVM and KNN. However, the GLCM features; GLCM [0 1], GLCM [-1 1], GLCM [-1 0], and GLCM [-1 -1] are used only for SVM.

As for the parameters selected for testing both LBP and the uniform rotation-invariant, which are adopted in this investigation, are eight neighbours (P = 8) and their relationship to the central pixel. Therefore, the number of bins is 59, following P(P-1) + 3. Additionally, this method is used to achieve rotation stability by combining identical, uniform patterns from different directions into a single bin. In contrast, the remaining patterns are placed in separate bins, resulting in a total of 10 distinct output bins (P + 2). The setting of LBP features is presented in **Table 4**.

Table 4. LBP features' setting.

Parameter	**Setting**		
Item	1	2	3
No. of neighbors (P)	8	8	8
Rotation Invariant	Yes (P+2)	No (P(P-1)+3)	custom normalization
Result	10 features	59 features	4248 features

For the multiclass classification using SVM, the models' one against all' and 'one against one' with a linear kernel are adopted. Concerning the classifier KNN, Euclidean distance is applied for measuring the distance between the test point and all reference points to obtain the K nearest neighbours, and the number of neighbours is set as k=1. To select the most preferable

combination of classifiers and feature extraction, the results are interpreted. The total accuracy, which shows the fraction of cases that are classified correctly, as well as precision and recall, are evaluated to support the selection.

Each of **Tables 5 and 6** summarizes the obtained results of the experimental evaluation, where the performance of each group of the classifier and methods of extracting features is evaluated using cross-validation k-fold which is the error estimator. In our current work, k=4 which means that the model is trained and evaluated four times repeatedly by randomly assigning four equal-sized subgroups to satisfy the necessary. In each attempt, the training of the system is performed using three of the subsets, whereas the remainder subset is used for evaluation or testing.

Table 5. Evaluation results of multiclass classification based on SVM.

Multiclass based on SVM learner	Accuracy (%)	Precision (%)	Recall (%)
GLCM [-2 2]	90.00	93.75	93.75
GLCM [0 2]	91.66	95.83	91.66
GLCM [-2 0]	90.90	93.75	95.00
GLCM [-2 -2]	90.00	93.75	93.75
GLCM both {[-2 2], [0 2]}	90.00	93.75	93.75
LBP 59 Features	87.50	91.66	91.66
LBP 10 Features	83.33	86.66	86.66

Table 6. Evaluation results of classification based on KNN.

KNN classifier	Accuracy (%)	Precision (%)	Recall (%)
GLCM [-2 2]	90.00	93.75	87.50
GLCM [0 2]	87.50	91.66	91.66
GLCM [-2 0]	90.00	93.75	87.50
GLCM [-2 -2]	90.00	93.75	87.50
GLCM {[-2 2], [0 2]}	87.50	91.66	91.66
LBP 59 Features	87.50	91.66	91.66
LBP 10 Features	75.00	75.00	79.17

The accuracy of the SVM classifier is higher compared with that of the k-Nearest Neighbour. Detailed results obtained by the various combinations of classifiers and features are presented in **Tables 7 and 8**. **Table 7** presents the value of the highest accuracy obtained when the GLCM technique is used to extract the features. Evaluating the 2-pixel neighbourhood to the east [0 2] on images leads to an accuracy value of 91.66%. Examining the neighborhood two pixels away in all directions yields high-accuracy results. Generally, extracted features by the use of GLCM show satisfactory results. With five tests, the achieved accuracy is 90% or higher, and the obtained precision and recall are also 90% or above.

Table 7. SVM multiclass classification results using GLCM features.

Multiclass based on SVM learner	Accuracy (%)	Precision (%)	Recall (%)
GLCM [-2 2]	90.00	93.75	93.75
GLCM [-1 1]	83.33	92.85	91.66
GLCM [0 2]	91.66	95.83	91.66
GLCM [0 1]	88.88	93.75	87.5
GLCM [-2 -2]	90.00	93.75	93.75
GLCM [-1 -1]	84.00	90.83	93.05
GLCM [-2 0]	90.90	93.75	95.00
GLCM [-1 0]	83.33	92.85	83.3
GLCM both {[-2 2], [0 2]}	90.00	93.75	93.75
GLCM both {[-1 1], [0 1]}	87.50	90.66	87.5

Combining both multiclass classifiers based on SVM and LBP features (as presented in **Table 8**) results in high accuracy when the rotation invariance of features is not considered. Thus, it can be concluded that rotation invariance reduces accuracy, as it causes the loss of certain informative features. Therefore, the use of invariant rotation features can enhance accuracy by approximately 83.33% compared with 87.5% when dispensing. In this case, the classifier demonstrates strong robustness, achieving a recall and precision of 91.66%.

Table 8. SVM multiclass classification results using LBP features.

Multiclass based on SVM learner	Accuracy (%)	Precision (%)	Recall (%)
LBP 59 Features	87.50	91.66	91.66
LBP 10 Features	83.33	86.66	86.66

Regarding the KNN classifier, several preliminary tests have been conducted to determine the optimal value for the neighbourhood dimension in this KNN classifier implementation. The conclusion reached is the best use of k=1. However, the best results with this classifier were inferior to those obtained by the SVM classifier. The combination of the KNN classifier and the GLCM features yields the best results, with an accuracy of 90%.

4. Conclusion and Future Work

In this paper, two machine learning approaches are proposed for detecting and classifying the defects of welding. These approaches are SVM and KNN. By using the dataset for training and testing strategies, the SVM shows higher results compared to the second classifier, KNN. However, the matching occurs between the stored data, which comes from the training and testing data, and is adopted by the KNN classifier. The high similarity that exists in the images of welding inspection, which leads to the closeness of many feature values, is one of the reasons that makes the low KNN accuracy. GLCM and LBP techniques are used for extracting the features. Using the LBP technique, the displacement value is adopted by the closely adjacent

neighbour. Using the GLCM technique, the second neighbour is adopted. Some future works can be pointed out as follows: 1) new software and methods can be used and assessed, 2) the current work is restricted to the spatial domain; therefore, the frequency domain can be considered, 3) investigating new and advanced supervised/unsupervised classifiers is recommended. 4) a new technique for extracting features is recommended for investigation and assessment, 5) expand the study to include all types of welding defects. Moreover, Expanding the dataset to include a larger number of images and a wider variety of welding defect types would improve generalization and classification reliability.

Author Contribution: All authors contributed equally to this paper. All authors read and approved the final paper.

Funding: This research received no external funding.

Conflicts of Interest: The authors declare no conflict of interest.

References:

[1] Kumar DD, Fang C, Zheng Y, Gao Y., Semi-supervised transfer learning-based automatic weld defect detection and visual inspection, Engineering Structures, 292:116580, 2023, https://doi.org/10.1016/j.engstruct.2023.116580

[2] Kadhim SJ, Al-Sabur RK, Ali ABK., Application of different median filter algorithms for welding defects clarification in radiographic images, Thi-Qar University Journal for Engineering Sciences, 11(1):56–61, 2020, https://doi.org/10.31663/tqujes.11.1.378(2020)

[3] Wang D, Yi Q, Liu Y, Lu R, Tian G., Advanced detection and reconstruction of welding defects in irregular geometries using eddy current pulsed thermography, NDT & E International, 154:103398, Sep. 2025, https://doi.org/10.1016/j.ndteint.2025.103398

[4] Alvarado JWV, García LFC, Neira MT, Flores JWV, Probability of Defects Detection in Welded Joints using the Magnetic Particle Method, Archives of Metallurgy and Materials, 69 (2):607-612, Mar. 2024, https://doi.org/10.24425/amm.2024.149789

[5] Sumardani NI, Setiawan NI, Nuryadin BW, Sumardani D., Defect Analysis of Carbonsteel Pipe Welding Connections Using Non-Destructive Testing with the Penetrant Test Method. Risenologi, 5(1):38–47, 28 April 2020, https://doi.org/10.47028/j.risenologi.2020.51.72

[6] Aboali A, El-Shaib M, Sharara A, Shehadeh M., Screening for welding defects using acoustic emission technique, Advanced Materials Research, 1025–1026:7–12, Sep. 2014, https://doi.org/10.4028/www.scientific.net/amr.1025-1026.7

[7] Alasdi SN, Al-Sabur R, In-Depth thermal analysis of different PIN configurations in friction stir spot welding of similar and dissimilar alloys, Journal of Manufacturing and Materials Processing, 9(6):184, Jun 2025, https://doi.org/10.3390/jmmp9060184

[8] Salgado-Lopez JM, Ojeda-Elizarrarás JL, Silva-Hernandez A, Tello-Rico JM., Failure of an autotank repaired by welding, Journal of Scientific and Technical Applications, 6(17): 1–9, http://doi.org/10.35429/jsta.2020.17.6.1.9

[9] Hamade RF, Baydoun AMR., Nondestructive detection of defects in friction stir welded lap joints using computed tomography, Materials & Design, 162:10–23, 2019, https://doi.org/10.1016/j.matdes.2018.11.034

[10] Abdelkader R, Ramou N, Khorchef M, Chetih N, Boutiche Y., Segmentation of x-ray image for welding defects detection using an improved Chan-Vese model, Materials Today Proceedings, 42(5): 2963–2967, 2021, https://doi.org/10.1016/j.matpr.2020.12.806

[11] Liao TW., Classification of weld flaws with imbalanced class data, Expert Systems With Applications, 35(3):1041–52, August 2008, https://doi.org/10.1016/j.eswa.2007.08.044

[12] Chen Y, He Y, Wu L., Detection of welding defects using the YOLOV8-ELA algorithm, Applied Sciences, 15(9):5204, May 2025, https://doi.org/10.3390/app15095204

[13] Orlando M, De Maddis M, Razza V, Lunetto V., Non-destructive detection and analysis of weld defects in dissimilar pulsed GMAW and FSW joints of aluminium castings and plates through 3D X-ray computed tomography, The International Journal of Advanced Manufacturing Technology, 132(5–6):2957–70, April 2024, https://doi.org/10.1007/s00170-024-13576-x

[14] Liao TW, Ni J., An automated radiographic NDT system for weld inspection: Part I — Weld extraction, NDT & E International, 29(3):157–62, June 1996, https://doi.org/10.1016/0963-8695(96)00009-6

[15] Da Silva RR, Calôba LP, Siqueira MHS, Rebello JMA., Pattern recognition of weld defects detected by radiographic test, NDT & E International, 37(6):461–70, Feb 2004, https://doi.org/10.1016/j.ndteint.2003.12.004

[16] Tou J. Y. and Lau P. Y., Gabor Filters and Grey-level Co-occurrence Matrices in Texture Classification, MMU International Symposium on Information and Communications Technologies, pp. 197–202, 2007

[17] Valentin P, Kounalakis T, Nalpantidis L., Weld Classification Using Gray Level Co-Occurrence Matrix and Local Binary Patterns, IST 2018 - IEEE International Conference on Imaging Systems and Techniques, pp. 1-6, Oct 2018, https://doi.org/10.1109/ist.2018.8577092

[18] Abidin Z, Anompa MA, Muhtadan., Development of welding defects identifier application on radiographic film using gray level co-occurrence matrix and backpropagation, AIP Conference Proceedings, 70–74, Jan 2013, https://doi.org/10.1063/1.4820996

[19] Ramana EV, Penekalapati SV, Namala KK., Identification of weld sub-surface defects by radiographic images using texture features, E3S Web of Conferences, 552:01017, Jan 2024, https://doi.org/10.1051/e3sconf/202455201017

[20] Mery D, Berti MA., Automatic detection of welding defects using texture features, Insight - Non-Destructive Testing and Condition Monitoring, 45(10):676–81, Oct 2003, https://doi.org/10.1784/insi.45.10.676.52952

[21] Wang X., Wong B.S., Tan C. S., Recognition of welding defects in radiographic images by using support vector machine classifier, Research Journal of Applied Sciences, Engineering and Technology, 2(3): 295-301, 2010.

[22] Hassan J, Awan AM, Jalil A., Welding Defect Detection and Classification Using Geometric Features. In Proceedings - 10th International Conference on Frontiers of Information Technology, FIT 2012, pp. 139–44, 2012, https://doi.org/10.1109/fit.2012.33

[23] Valavanis I, Kosmopoulos D., Multiclass defect detection and classification in weld radiographic images using geometric and texture features, Expert Systems With Applications, 37(12):7606–14, May 2010, https://doi.org/10.1016/j.eswa.2010.04.082

[24] Palma-Ramírez D, Ross-Veitía BD, Font-Ariosa P, Espinel-Hernández A, Sanchez-Roca A, Carvajal-Fals H, et al., Deep convolutional neural network for weld defect classification in radiographic images, Heliyon, 10(9):e30590, May 2024, https://doi.org/10.1016/j.heliyon.2024.e30590

[25] Zhang W, Liu W, Yu X, Kang D, Xiong Z, Lv X, et al., Deep Learning-Based Automated Detection of welding defects in Pressure Pipeline radiograph, Coatings, 15(7):808, July 2025, https://doi.org/10.3390/coatings15070808

[26] Lone AH, Siddiqui AN, Noise models in digital image processing, Global Sci-Tech, 10(2):63, 2018, https://doi.org/10.5958/2455-7110.2018.00010.1

[27] Singh H, Kaur S, Sharma P, Utilizing Various Filtering Methodologies in Digital Image Processing, 2024 International Conference on Electrical Electronics and Computing Technologies (ICEECT), Greater Noida, India: IEEE, 1–6, Aug 2024, https://doi.org/10.1109/iceect61758.2024.10738905

[28] Al-taie R., Saleh B., Abu-Alsaad H., A REVIEW PAPER: DIGITAL IMAGE FILTERING PROCESSING, 3(9): 1-11, 2021, https://doi.org/10.47577/technium.v3i9

[29] Rivera-Aguilar BA, Cuevas E, Luque-Chang A, López J, Pérez-Cisneros M., Pixel Interaction model for contrast enhancement: bridging social science and image processing, Applied Sciences, 14(23):10887, 2024, https://doi.org/10.3390/app142310887

[30] Patel P, Bhandari A., A review on image contrast enhancement techniques, SMART MOVES JOURNAL IJOSCIENCE, 5(7):18-22, Jul 2019, https://doi.org/10.24113/ijoscience.v5i7.217, https://scispace.com/pdf/a-review-on-image-contrast-enhancement-techniques-mn53j9lvgm.pdf

[31] Lasnel R, Frouté L, Kovscek AR, Jolivet IC, Creux P., Image processing and segmentation open source codes applied to FIB-SEM images of ultra-tight gas shales samples: Enhanced pore space representativeness and mineral identification, Gas Science and Engineering, 138:205610, March 2025, https://doi.org/10.1016/j.jgsce.2025.205610

[32] Mageswari SU, Sridevi M, Mala C., An experimental study and analysis of different image segmentation techniques, Procedia Engineering, 64:36–45, Jan 2013, https://doi.org/10.1016/j.proeng.2013.09.074

[33] Atta MA, Imtiaz M, Hassan A, Saqib S., Image segmentation by using threshold techniques, Lahore Garrison University Research Journal of Computer Science and Information Technology, 2(2):1–6, 2018, https://lgurjcsit.lgu.edu.pk/index.php/lgurjcsit/issue/view/29/18

[34] Chen X, Liu C, Xie D, Miao D., Image thresholding segmentation method based on adaptive granulation and reciprocal rough entropy, Information Sciences, 695:121737, March 2025, https://doi.org/10.1016/j.ins.2024.121737

[35] Haralick RM, Shanmugam K, Dinstein I., Textural features for image classification, IEEE Transactions on Systems Man and Cybernetics, SMC-3(6):610–621, Nov 1973, https://doi.org/10.1109/tsmc.1973.4309314

[36] Utaminingrum F, Alqadri AM, Somawirata IK, Karim C, Septiarini A, Lin CY, et al., Feature selection of gray-level Cooccurrence matrix using genetic algorithm with Extreme learning machine classification for early detection of Pole roads, Results in Engineering, 20:101437, Sep 2023, https://doi.org/10.1016/j.rineng.2023.101437

[37] Iqbal N, Mumtaz R, Shafi U, Zaidi SMH., Gray level co-occurrence matrix (GLCM) texture based crop classification using low altitude remote sensing platforms, PeerJ Computer Science, 7:1-26, May 2021, https://doi.org/10.7717/peerj-cs.536

[38] Jobanputra R, Clausi DA., Preserving boundaries for image texture segmentation using grey level co-occurring probabilities, Pattern Recognition, 39(2):234–245, 2006, https://doi.org/10.1016/j.patcog.2005.07.010

[39] Kwak JT, Xu S, Wood BJ., Efficient data mining for local binary pattern in texture image analysis, Expert Systems With Applications, 42(9):4529–4539, Feb 2015, https://doi.org/10.1016/j.eswa.2015.01.055

[40] Lan S, Liao X, Fan H, Hu S, Pan Z., A multi-channel framework based Local Binary Pattern with two novel local feature descriptors for texture classification., Digital Signal Processing, 140:104124, 2023, https://doi.org/10.1016/j.dsp.2023.104124

[41] Kaur N., Nazir N., Manik, A Review of Local Binary Pattern Based texture feature extraction, 2021 9th International Conference on Reliability, Infocom Technologies and Optimization (Trends and Future Directions) (ICRITO), Noida, India: IEEE, 2021, https://doi.org/10.1109/ICRITO51393.2021.9596485

[42] Ojala T, Pietikäinen M, Harwood D., A comparative study of texture measures with classification based on featured distributions, Pattern Recognition, 29(1):51–59, 1996, https://doi.org/10.1016/0031-3203(95)00067-4

[43] Ojala T, Pietikäinen M, Mäenpää T., Gray Scale and Rotation Invariant Texture Classification with Local Binary Patterns, In: Lecture notes in computer science, 1842: 404–420, 2000, https://doi.org/10.1007/3-540-45054-8_27

[44] Ikram K, Djilali K, Abdennasser D, Al-Sabur R, Ahmed B, Sharkawy AN., Comparative analysis of fouling resistance prediction in shell and tube heat exchangers using advanced machine learning techniques, Research on Engineering Structures and Materials, 10(1): 253-270, 2024, https://doi.org/10.17515/resm2023.858en0816

[45] Shi B, Liu J., Nonlinear metric learning for kNN and SVMs through geometric transformations, Neurocomputing, 318:18–29, Aug 2018, https://doi.org/10.1016/j.neucom.2018.07.074

[46] Fan Z, Xie JK, Wang ZY, Liu PC, Qu SJ, Huo L., Image classification method based on improved KNN algorithm, Journal of Physics Conference Series, 1930(1):012009, May 2021, https://doi.org/10.1088/1742-6596/1930/1/012009

[47] Allwein E.L., Schapire R.E., Singer Y., Reducing Multiclass to Binary: A Unifying Approach for Margin Classifiers Erin, Journal of Machine Learning Research, 1: 113-141, 2000, https://www.jmlr.org/papers/volume1/allwein00a/allwein00a.pdf

[48] Liu Y, Bi JW, Fan ZP., A method for multi-class sentiment classification based on an improved one-vs-one (OVO) strategy and the support vector machine (SVM) algorithm, Information Sciences, 394–395:38–52, 2017, https://doi.org/10.1016/j.ins.2017.02.016

[49] Bahedh AS, Mishra A, Al-Sabur R, Jassim AK., Machine learning algorithms for prediction of penetration depth and geometrical analysis of weld in friction stir spot welding process, Metallurgical Research & Technology, 119(3):305, Jan 2022, https://doi.org/10.1051/metal/2022032

[50] Al-Sabur R, Mishra A, Khalaf HI., Mastering friction stir welding (FSW) with Machine Learning (ML): A Comprehensive Guide to Algorithms and Applications, In book: Using Computational Intelligence for Sustainable Manufacturing of Advanced Materials, 387–416, 2025, https://doi.org/10.4018/979-8-3693-7974-5.ch017

[51] Encord Computer Vision Glossary, “Confusion Matrix,” ENCORD. Accessed: Sep. 02, 2025. [Online]. Available: https://encord.com/glossary/confusion-matrix/

[52] Sokolova M, Lapalme G., A systematic analysis of performance measures for classification tasks, Information Processing & Management, 45(4):427–37, May 2009, https://doi.org/10.1016/j.ipm.2009.03.002

[53] Mahmoud KH, Abdel-Jaber GT, Sharkawy AN., Neural Network-Based Classifier for collision classification and identification for a 3-DOF industrial robot, Automation, 5(1):13–34, 2024, https://doi.org/10.3390/automation5010002